Zitterbewegung in bilayer graphene: effects of trigonal warping and electric field

Eylee Jung[1], DaeKil Park[2,3] and Chang-Soo Park[4*]

[1]*Center for Superfunctional Materials, Department of Chemistry, Pohang University of Science and Technology, Pohang 790-784, Republic of Korea*

[2]*Department of Physics, Kyungnam University, Changwon, 631-701, Republic of Korea*

[3]*Department of Electronic Engineering, Kyungnam University, Changwon, 631-701, Republic of Korea*

[4] *Department of Physics, Dankook University, Cheonan, 330-714, Republic of Korea*

(Dated: March 17, 2013)

Abstract

We study the effects of trigonal warping and electric field on the Zitterbewegung of low-energy electrons in bilayer graphene. A time-dependent average velocity of electrons is calculated by using Gaussian wave packets. The Zitterbewegung of electric current shows a transient behavior. The anisotropy of eigenspectrum due to the trigonal warping distortion breaks the valley symmetry to induce valley-polarized Zitterbewegungs of electric current. An external electric field, applied perpendicular to the layer, opens a bandgap and makes the group velocities of electrons at conduction and valence bands slower. Using this feature we demonstrate that the decay time of the transient Zitterbewegung can be made longer by the electric field. Combining these effects it is expected that valley-polarized Zitterbewegungs of electric current with longer decay time, which eventually become two valley-polarized constant currents at large times, can exist in a biased bilayer graphene with trigonal warping.

PACS numbers: 73.22.Pr, 72.80.Vp, 03.65.Pm

I. INTRODUCTION

The search for the Zitterbewegung (ZB), a highly oscillatory motion of a relativistic particle due to the interference between positive- and negative-energy states in a wave packet,[1–4] of nonrelativistic particles in solids has been of interest for years. Since the phenomenon requires positive and negative states solids with two-band energy spectrum were proposed as possible candidates,[5] and many such systems have been studied in this direction.[6–15] More recently, carbon based two-dimensional systems, namely, monolayer and bilayer graphene have also been attracted for the investigation of the ZB.[16–19] In the absence of external field both systems have gapless two-band energy spectrum,[20–23] and hence one can expect the ZB phenomenon in these systems. Rusin and Zawadzki[18] demonstrated, using Gaussian wave packets, that the ZB in monolayer and bilayer graphene is transient with decay time of femtoseconds. In particular, owing to the quadratic dispersion of the energy eigenspectrum, they were able to obtain analytical results of the ZB in bilayer graphene (BLG). In their study the authors employed a simplified effective low-energy Hamiltonian, including only the intralayer hopping and strong interlayer coupling energies, so that the eigenspectrum has a parabolic dispersion and the Fermi surface displays isotropic energy contours. According to McCann and Fal'ko,[24] however, the low-energy Hamiltonian of BLG can include the weak interlayer coupling energy that induces a trigonal warping (TW) energy distortion and, in the presence of an external electric field, an interlayer potential energy difference term can also be incorporated. Although the energy spectrum is dominated by the parabolic dispersion these terms can play important roles in the dynamics of the low-energy electrons in BLG.[25–27]

In this paper we take account of the trigonal warping and an external electric field to examine their effects on the ZB in BLG. The TW term deforms the isotropic energy to break the symmetry between K and K' valleys.[24,28] In the presence of an external electric field, applied perpendicular to the BLG layers (*biased* BLG), an electrostatic potential asymmetry between the two layers is induced, as a result of which a bandgap opens in the energy spectrum.[29–34] The main effects of these two quantities on the ZB then appear as valley-polarized ZB's due to the symmetry breaking energy distortion and longer decay time of the transient ZB due to the electric field, making the observation of the ZB in a biased BLG more feasible. We demonstrate these effects explicitly by calculating a time-dependent average velocity of low-energy electrons with Gaussian wave packets.

The paper is organized as follows. In the following section we present energy eigenspectrum of

the biased BLG with the TW distortion. The characteristics of the eigenspectrum will be qualitatively analyzed in connection with the ZB. We also derive a time-dependent average velocity using a Gaussian wave packet, which is described by integrals over the momentum distribution of the packet. Although a full analysis of the ZB requires numerical calculations due to the non-trivial dispersion relation of the eigenspectrum many important features about the ZB oscillation and its valley dependency can be predicted from the derived form. In Sec. III, using the obtained average velocity, we numerically calculate time-dependent electric currents and show valley-polarized ZB's and lengthening of the decay time of the transient ZB, together with relevant discussions. Finally there will be a summary in Sec. IV.

II. LOW-ENERGY EIGENSPECTUM AND TIME-DEPENDENT AVERAGE VELOCITY

A. Energy eigenspectrum

We start with the low-energy effective Hamiltonian of a BLG applied by an external electric field perpendicular to the layer,[24]

$$\hat{\mathcal{H}} = \begin{pmatrix} \tau\left(u - \frac{1}{2m_u}\hat{\pi}^\dagger\hat{\pi}\right) & -\frac{1}{2m^*}(\hat{\pi}^\dagger)^2 + \tau v_3\hat{\pi} \\ -\frac{1}{2m^*}\hat{\pi}^2 + \tau v_3\hat{\pi}^\dagger & -\tau\left(u - \frac{1}{2m_u}\hat{\pi}\hat{\pi}^\dagger\right) \end{pmatrix}, \tag{1}$$

where $\hat{\pi} = \hat{p}_x + i\hat{p}_y$ ($\hat{p}_{x,y} = -i\hbar\partial_{x,y}$), $m^* = \gamma_1/2v_F^2$ is an effective mass with the Fermi velocity v_F[35] and $\gamma_1 \approx 0.4$ eV being the interlayer hopping energy between A and $\tilde{B}$ atoms, and τ is the valley index with $\tau = +1$ for K-valley and $\tau = -1$ for K'-valley. The effective velocity v_3 is related to the weak interlayer coupling energy $\gamma_3 \approx 0.3$ eV and given as $v_3 = \gamma_3 v_F/\gamma_0 = 0.107 v_F$ with $\gamma_0 \approx 2.8$ eV being the intralayer hopping energy between A and B atoms. The parameter u is half of the interlayer electrostatic energy difference (or asymmetry in short) due to the applied electric field; associated with this parament another effective mass $m_u = \gamma_1^2/2uv_F^2$ is introduced for subsequent use. This Hamiltonian is valid in the energy range $|E| \lesssim \gamma_1/4$ (≈ 0.1 eV).

The low-energy eigenspectrum of the Hamiltonian, satisfying $\hat{\mathcal{H}}|\varphi_{\tau s}(\boldsymbol{k})\rangle = E_{\tau s}(\boldsymbol{k})|\varphi_{\tau s}(\boldsymbol{k})\rangle$, is

$$\begin{aligned} &E_{\tau s}(\boldsymbol{k}) = sE_\tau, \quad E_\tau = \sqrt{\epsilon_k^2 + \epsilon_{3k}^2 - 2\tau\epsilon_k\epsilon_{3k}\cos 3\phi + (u-\epsilon_u)^2}, \\ &\epsilon_k = \frac{\hbar^2k^2}{2m^*}, \quad \epsilon_{3k} = \hbar k v_3, \quad \epsilon_u = \frac{\hbar^2k^2}{2m_u}, \quad \phi = \arctan\frac{k_y}{k_x}. \end{aligned} \tag{2}$$

Here, s is the band index with $s = +1$ and $s = -1$ for conduction band and valence band, respectively. This eigenspectrum is valid in the energy range $\epsilon^* \lesssim |E| \lesssim 0.1$ eV with ϵ^* being the Lifshitz transition energy.[36] The corresponding plane wave (pseudo)eigenspinor, taking the δ-function normalization, has the form

$$\varphi_{\tau s}(\boldsymbol{r}) = \frac{1}{\sqrt{2E_\tau}} \begin{pmatrix} \sqrt{E_\tau + \tau s(u - \epsilon_u)} \\ \\ -s\sqrt{E_\tau - \tau s(u - \epsilon_u)}\, e^{i\delta_\tau} \end{pmatrix} \frac{e^{i\boldsymbol{k}\cdot\boldsymbol{r}}}{2\pi},$$
$$\delta_\tau(k, \phi) = \arctan \frac{\epsilon_k \sin 2\phi + \tau\epsilon_{3k} \sin\phi}{\epsilon_k \cos 2\phi - \tau\epsilon_{3k} \cos\phi}, \tag{3}$$

where $\varphi_{\tau s}(\boldsymbol{r}) = \langle \boldsymbol{r}|\varphi_{\tau s}(\boldsymbol{k})\rangle$ and $\boldsymbol{k} = (k_x, k_y)$ are 2D wave vectors.

In the absence of ϵ_{3k} and external electric field (*unbiased* BLG) the eigenspectrum reduces to $E_{\tau s}(\boldsymbol{k}) = s\hbar^2k^2/2m^*$; it has a parabolic dispersion at each band and the isoenergy (the Fermi energy) contour is isotropic. Including the terms involving ϵ_{3k} in Eq. (2) the eigenspectrum is deformed, resulting in an anisotropic dispersion with trigonal warping (see Fig. 1(a)): Note the high-anisotropy energy dispersion at $E = 0.25\gamma_1 \approx 0.1$ eV, which confirms one should consider the TW distortion in the valid energy range of $|E| \lesssim 0.1$ eV. This TW distortion then makes the energy dispersions at K and K' valleys different as illustrated Fig. 1(c), that is, the valley symmetry is broken. Now, when an external electric field is applied to this BLG an interlayer asymmetry is induced, which in turn opens a gap between the conduction and valence bands (see Fig. 1(b)); the biased BLG is a semiconductor with tunable bandgap by the external electric field.

In connection with the ZB in a BLG the effects of the anisotropic dispersion due to the TW distortion and the opening of a bandgap can be explained as follows. For this and subsequent use we first define a momentum-dependent group velocity

$$\boldsymbol{v}_{\tau s}(\boldsymbol{k}) = s\boldsymbol{v}_{g\tau}(\boldsymbol{k}), \quad \boldsymbol{v}_{g\tau}(\boldsymbol{k}) = \frac{1}{\hbar}\nabla_{\boldsymbol{k}} E_\tau(\boldsymbol{k}), \tag{4}$$

where $\nabla_{\boldsymbol{k}} = \partial_{k_x}\mathbf{e}_x + \partial_{k_y}\mathbf{e}_y$. As depicted in Fig. 1(c), since the curvature of an anisotropic contour varies the group velocities $\boldsymbol{v}_{g\tau}(\boldsymbol{k})$ for a given wave vector $\boldsymbol{k}$ are different at K and K' valleys. This valley-dependent velocities then yield valley-polarized ZB's of electric currents as we shall show in numerical results. Next, to see the effect of the gap opening we look into the band diagram plotted in Fig. 1(b); the variation of energy dispersion in the biased case (the solid lines) is smaller than that in the unbiased case (the dashed lines). Consequently, the group velocities at each band become slower, which then leads to longer duration of the transient ZB in the biased BLG compared to the unbiased case.

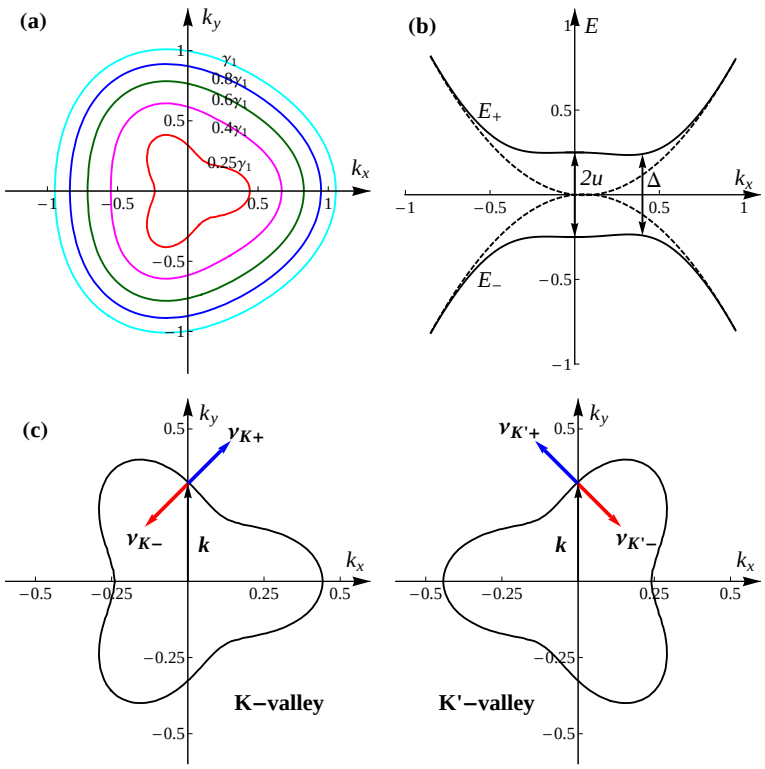

FIG. 1: (Color online) In all plots, the wave vectors are in unit of $\gamma_1/\hbar v_F = 6.73 \times 10^8$ m^{-1} and the energy is in unit of γ_1. (a) K-valley energy contours when $u = 0.25\gamma_1$. A clear anisotropic dispersion with trigonal warping can be seen at $E = 0.25\gamma_1$. The higher energy contours are plotted for illustrative purpose. (b) The corresponding energy band diagram along the line $k_y = 0$ with interlayer asymmetry $2u = 0.5\gamma_1$ and band gap $\Delta(\approx 2u)$. The dashed line shows the case $u = 0$. (c) Schematic of the isoenergy contours for K and K' valleys when $E = 0.25\gamma_1$ and $u = 0.25\gamma_1$ and the group velocities (in arbitrary unit) $\boldsymbol{v}_{\tau s}(\boldsymbol{k}) = s\boldsymbol{v}_{g\tau}(\boldsymbol{k})$ (see text). Note the velocities of two valleys corresponding to the same wave vector $\boldsymbol{k}$ are different and, at each valley, the conduction- and valence-band velocities ($\boldsymbol{v}_{\tau+}$ and $\boldsymbol{v}_{\tau-}$) are opposite to each other.

B. Time-dependent average velocity

Having obtained the eigenspectrum and eigenspinor we derive a time-dependent average velocity[38] of electrons in the biased BLG with TW. For this purpose we use a two-dimensional Gaussian wave packet whose initial state is

$$|\psi_\tau(0)\rangle = \sum_{s=\pm} |\psi_{\tau s}(0)\rangle, \quad |\psi_{\tau s}(0)\rangle = \int d^2\boldsymbol{k}\, a_{\tau s}(\boldsymbol{k})\, |\varphi_{\tau s}(\boldsymbol{k})\rangle, \tag{5}$$

where $a_{\tau s}(\boldsymbol{k})$ is the 2D momentum amplitude with width $2\sqrt{2}/d$ and mean momentum $\hbar\boldsymbol{k}_0 = (\hbar k_{0x}, \hbar k_{0y})$, given as[39]

$$a_{\tau s}(\boldsymbol{k}) = \frac{\sqrt{E_\tau + \tau s(u - \epsilon_u)}}{\sqrt{2E_\tau}} A(\boldsymbol{k}),$$
$$A(\boldsymbol{k}) = \frac{d}{\sqrt{\pi}}\, e^{-d^2(k_x - k_{0x})^2/2} e^{-d^2(k_y - k_{0y})^2/2}. \tag{6}$$

With this choice of wave packet the time-dependent average velocity, in Schrödinger picture, can be defined as (see also Appendix A)

$$\boldsymbol{v}_\tau(t) = \langle\psi_\tau(t)|\, \hat{\boldsymbol{v}}\, |\psi_\tau(t)\rangle, \quad \hat{\boldsymbol{v}} = \frac{1}{i\hbar}\left[\hat{\boldsymbol{r}}, \hat{\mathcal{H}}\right], \tag{7}$$

where $\hat{\boldsymbol{r}} = (\hat{x}, \hat{y})$ and the time-evolution state can be obtained from $|\psi_\tau(t)\rangle = \exp[-i\hat{\mathcal{H}}t/\hbar]|\psi_\tau(0)\rangle$. Using this definition and the eigenspinor in Eq. (3), with the help of the relation $\hat{\mathcal{H}}|\varphi_{\tau s}(\boldsymbol{k})\rangle = sE_\tau(\boldsymbol{k})|\varphi_{\tau s}(\boldsymbol{k})\rangle$, we find

$$\boldsymbol{v}_\tau(t) = \int d^2\boldsymbol{k}\, |A(\boldsymbol{k})|^2 \left[v_{\tau x}(\boldsymbol{k}, t)\, \mathbf{e}_x + v_{\tau y}(\boldsymbol{k}, t)\, \mathbf{e}_y\right], \tag{8}$$

where $v_{\tau x}(\boldsymbol{k}, t)$ and $v_{\tau y}(\boldsymbol{k}, t)$ are given as

$$\begin{aligned}
v_{\tau x}(\boldsymbol{k}, t) &= v_{x0} + v_{x1}\cos\left(\frac{2E_\tau}{\hbar}t\right) + v_{x2}\sin\left(\frac{2E_\tau}{\hbar}t\right) \\
v_{x0} &= \tau\frac{u}{E_\tau}(1 - \lambda^2k^2)v_{g\tau x}(\boldsymbol{k}), \\
v_{x1} &= -2\tau\frac{u}{\gamma_1}\lambda k_x v_F - v_{x0}, \\
v_{x2} &= \frac{\gamma_1}{E_\tau}\left(2\lambda^2k^2 - r^2 + 2\tau r\lambda k_x\right)\lambda k_y v_F, \\
v_{\tau y}(\boldsymbol{k}, t) &= v_{y0} + v_{y1}\cos\left(\frac{2E_\tau}{\hbar}t\right) + v_{y2}\sin\left(\frac{2E_\tau}{\hbar}t\right) \\
v_{y0} &= \tau\frac{u}{E_\tau}(1 - \lambda^2k^2)v_{g\tau y}(\boldsymbol{k}), \\
v_{y1} &= -2\tau\frac{u}{\gamma_1}\lambda k_y v_F - v_{y0}, \\
v_{y2} &= -\frac{\gamma_1}{E_\tau}\left[(2\lambda^2k^2 - r^2)\lambda k_x - \tau r\lambda^2(k_x^2 - k_y^2)\right]v_F.
\end{aligned} \tag{9}$$

In the above equations, $v_{g\tau(x,y)}(\boldsymbol{k})$ are the x and y components of group velocity defined in (4), $k^2 = k_x^2 + k_y^2$, $\lambda = \hbar v_F/\gamma_1 = 1.485$ nm, and $r = \gamma_3/\gamma_0 = 0.107$ is the dimensionless TW parameter.

The 2D integral in (8) involves integrands with non-trivial dependence on the wave vector $\boldsymbol{k}$, which requires numerical calculations. However, some important features about the ZB of velocity can be deduced from the above expressions . We first note that the average velocity $\boldsymbol{v}_\tau(t)$ depends

on the TW parameter r and the bandgap parameter u to which the valley index τ is tied. It is also seen from Eq. (9) that the first terms v_{x0} and v_{y0} represent the constant motion and the oscillatory ZB is conceived in the second (v_{x1}, v_{y1}) and third (v_{x2}, v_{y2}) terms. Thus, when $u \neq 0$ and $r \neq 0$, one should expect the ZB's as well as the constant velocity for both of the x and y components. In addition, they will have different values at K and K' valleys; see Appendix B for the discussion of the valley dependency of $\boldsymbol{v}_\tau(t)$. We emphasize here that these effects always exist in the biased BLG with TW, regardless of the choice of the initial mean momentum of the Gaussian wave packet. As an extreme example, both the constant velocity and the ZB can be present even for the choice of zero initial mean momentum $\hbar\boldsymbol{k}_0 = (0, 0)$; in this case the x-component constant velocity from v_{x0} and the y-component ZB oscillation due to v_{y2} exist. In other words, even if the initial Gaussian wavepacket has zero mean momentum, one can still expect the ZB oscillation of velocity in BLG when the energy eigenspectrum is deformed to have anisotropic dispersion. This is in sharp contrast to the case of unbiased BLG without TW (i.e., when $u = 0$ and $r = 0$) studied in Ref. 18, in which case no constant velocity appears and the ZB can occur only when $\hbar\boldsymbol{k}_0 \neq 0$.

Incidentally, we can predict other interesting results from Eq. (9). First, when $u = 0$ and $r \neq 0$ (the unbiased case but including the TW term), only the ZB oscillations appear because all terms vanish except the third terms v_{x2} and v_{y2}; this holds for any choice of $\hbar\boldsymbol{k}_0$. Second, when $u \neq 0$ and $r = 0$ (the biased case without considering the TW term), the existence of the constant velocity and the ZB depends on the choice of $\hbar\boldsymbol{k}_0$. From these analyses one can conclude that the inclusion of the TW term guarantees the existence of the ZB of velocity in BLG; as an extreme case, when $u = 0$ and $r \neq 0$ and for the choice of $\hbar\boldsymbol{k}_0 = (0, 0)$, the y-component ZB oscillation can exist. In the following section, by choosing a non-zero $\hbar\boldsymbol{k}_0$, we present numerical results of the ZB of velocity based on the above equations.

III. NUMERICAL RESULTS AND DISCUSSION

To discuss the ZB of velocity in the biased BLG with the TW distortion we calculate an electric current $\boldsymbol{j}_\tau(t) = e\boldsymbol{v}_\tau(t)$ by using the Gaussian wave packet with initial spacial width $d = 30$ nm and mean momentum $\hbar\boldsymbol{k}_0 = (0, \hbar k_{0y})$; for convenience we use $+e$ for the electric charge (thus, the actual currents should be the negative of the numerical results).

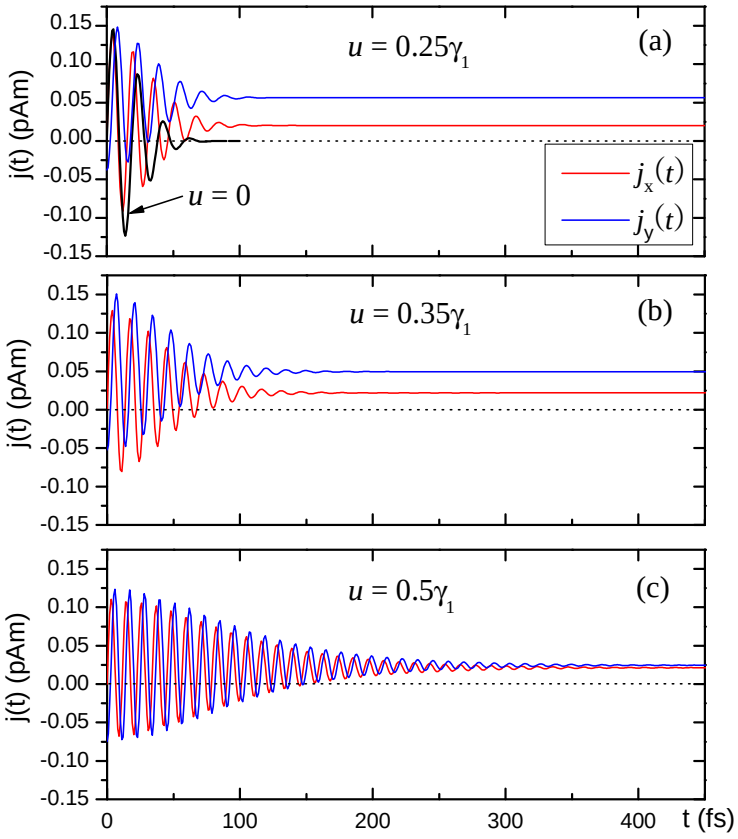

FIG. 2: (Color online) Zitterbewegung of the K-valley electric current $\boldsymbol{j}_K(t) = e\boldsymbol{v}_K(t)$ for different values of u when $\boldsymbol{k}_0 = (0,\ 0.35\ \mathrm{nm}^{-1})$ and $d = 30$ nm. The red and blue lines are the x and y components, respectively. The black line in (a) displays the unbiased case without the TW term, that is, when $u = 0$ and $\gamma_3 = 0$.

A. Effect of electric field

We first examine the effect of the opening of a bandgap due to the applied electric field. In Fig. 2 we plot the x (red line) and y (blue line) components of the K-valley electric current $\boldsymbol{j}_K(t) = e\boldsymbol{v}_K(t)$ for different values of u when $\boldsymbol{k}_0 = (0,\ 0.35\ \mathrm{nm}^{-1})$. Two features can be immediately observed from the results. First, the centers of the ZB oscillations are shifted to positive values, so that there exist non-zero constant electric currents at large times; on the contrary, there is no shift in the case of unbiased BLG (see the black line in Fig. 2(a)). As mentioned above this is expected from the constant velocity terms v_{x0} and v_{y0} in Eq. (9) which can have non-zero values when $u \neq 0$; the amount of shift is thus determined by these quantities. Since $r \neq 0$ in the present case the non-zero average velocities can exist even when the initial wave packet is at rest, (i.e.,

when $\hbar \boldsymbol{k}_0 = 0$). One can thus produce net constant currents as well as the ZB oscillation in the BLG with TW by applying an electric field perpendicular to the layer. This is reminiscent of the remnant displacement in the ZB of position discussed in Ref. 4 which, however, requires spherically asymmetric initial momentum distribution. In addition to the shifts, since the average velocities depend on the valley index, the constant electric currents will also be different at each valley. We shall come to this effect later in association with the valley-polarized ZB's.

Second, as in the unbiased BLG the ZB is transient,[18] which has been explained mathematically by using the Riemann-Lebesques theorem.[4] However, the decay time becomes longer as u increases (i.e., as the bandgap increases). This can be related to the decrease of group velocity in the biased BLG. To see this effect more clearly we use the similar reasoning discussed in Ref. 18; the decay time of the transient ZB can be associated with the relative velocity between the conduction- and valence-band wave packets. For the biased BLG with TW we calculate an average relative velocity between the two subpackets. First, the average velocity of subpacket at each band can be defined as

$$\begin{aligned} \langle \boldsymbol{v} \rangle_{\tau s} &= \langle \psi_{\tau s}(t) | \, \hat{\boldsymbol{v}} \, | \psi_{\tau s}(t) \rangle \quad (s = \pm) \\ &= \frac{1}{2} \int d^2 \boldsymbol{k} \, |A(\boldsymbol{k})|^2 \left(s + \tau \frac{u - \epsilon_u}{E_\tau} \right) \boldsymbol{v}_{g\tau}(\boldsymbol{k}), \end{aligned} \tag{10}$$

where $\epsilon_u = \hbar^2 k^2 / 2 m_u$ is given in Eq. (2) and $\boldsymbol{v}_{g\tau}(\boldsymbol{k})$ is the momentum-dependent group velocity defined in (4). From this the average relative velocity can be obtained as

$$\boldsymbol{v}^\tau_{rel} = \langle \boldsymbol{v} \rangle_{\tau +} - \langle \boldsymbol{v} \rangle_{\tau -} = \int d^2 \boldsymbol{k} \, |A(\boldsymbol{k})|^2 \boldsymbol{v}_{g\tau}(\boldsymbol{k}). \tag{11}$$

It can be seen from Eq. (10) that, unlike the group velocities of the two bands which are opposite to each other as illustrated in Fig. 1(c), the average velocities of the subpackets, $\langle \boldsymbol{v} \rangle_{\tau +}$ and $\langle \boldsymbol{v} \rangle_{\tau -}$, are not opposite to each other due to the second term in the integrand which depends on both the valley index and the gap parameter u (see also Eq. (12) below). We however note that the average relative velocity $\boldsymbol{v}^\tau_{rel}$ is described by the average of group velocities over the momentum distribution of the Gaussian wave packet; it is directly related to the group velocity. We also note that the relative velocity depends on the valley index τ. For the present choice of the initial mean momentum $\hbar \boldsymbol{k}_0 = (0, \hbar k_{0y})$, the x component is antisymmetric under the exchange of valley index, whereas the y component is symmetric (see Appendix B). Thus, the directions of $\boldsymbol{v}^K_{rel}$ and $\boldsymbol{v}^{K'}_{rel}$ are different, but they have the same magnitude of $v_{rel} = \left(v^2_{rel\,x} + v^2_{rel\,y} \right)^{1/2}$.

In Fig. 3 we plot the x and y components of $\boldsymbol{v}^\tau_{rel}$ (and also its magnitude v_{rel}) for K and K' valleys as a function of u/γ_1 when $k_{0y} = 0.35$ nm^{-1}: As to be discussed below the valid plot range

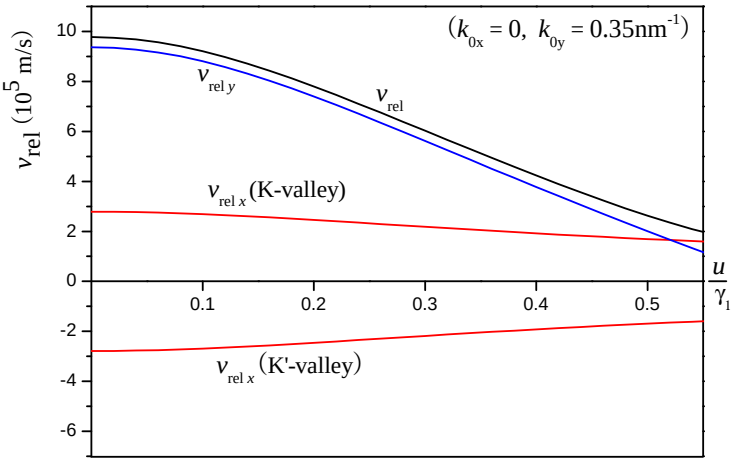

FIG. 3: (Color online) Average relative velocity $\boldsymbol{v}^{\tau}_{rel}$ and its components as a function of u/γ_1 when $d = 30$ nm and $\boldsymbol{k}_0 = (0, 0.35\ \text{nm}^{-1})$. v_{rel} (black line) is the magnitude of the relative velocity; $v_{rel} = \sqrt{v^2_{relx} + v^2_{rely}}$. Note there is no valley dependence in the y component, while the x components at K and K' valleys are opposite to each other (see Appendix B).

is $0 \lesssim u/\gamma_1 \lesssim 0.5$. It is seen that both the x and y components (and hence the magnitude v_{rel}) decrease as u increases. Obviously, this stems from the slower variation of the energy dispersion, that is, the decrease of group velocities when $u \neq 0$. As a numerical example, the decay time can be estimated as $t \sim d/v_{rel}$. The relative velocities, from numerical evaluation of the integral (11), are $v_{rel} = 2.9 \times 10^5$ m/s for $u = 0.5\gamma_1$ and $v_{rel} = 9.8 \times 10^5$ m/s for the unbiased case.[40] Thus, the corresponding decay times are, respectively, $t \sim 100$ fs and $t \sim 30$ fs, showing about three times large in the maximum biased case.

We have also checked the time variation of spacial width of the wave packet, that is, $|\Delta \boldsymbol{r}(t)|^2 = \langle \psi_{\tau s}(t)| \hat{\boldsymbol{r}}^2 |\psi_{\tau s}(t)\rangle - \langle \psi_{\tau s}(t)| \hat{\boldsymbol{r}} |\psi_{\tau s}(t)\rangle^2$ for different values of u to see if there exist any contractions of wave packets due to the anisotropic spectrum instead of spreading. For all values of u in the valid range $|\Delta \boldsymbol{r}(t)|$ always increases with small oscillations as time passes. Moreover, the spreading rate decreases as u increases, exhibiting little relevance of the spreading to the decay time. We thus believe the main reason for the lengthening of the decay time is the decrease of group velocities.

According to Ref. 28 the bandgap is tunable up to about $\Delta \sim \gamma_1$, that is, $u \sim 0.5\gamma_1$. Based on this, the valid range of u in the present analysis is approximately $0 \leq u \lesssim 0.5\gamma_1$. In order for the ZB to be appreciable in a biased BLG the energy uncertainty of electrons should be larger than the bangap, so that $u \lesssim \Delta E/2$. Considering the maximum case, $u = 0.5\gamma_1$, the corresponding energy

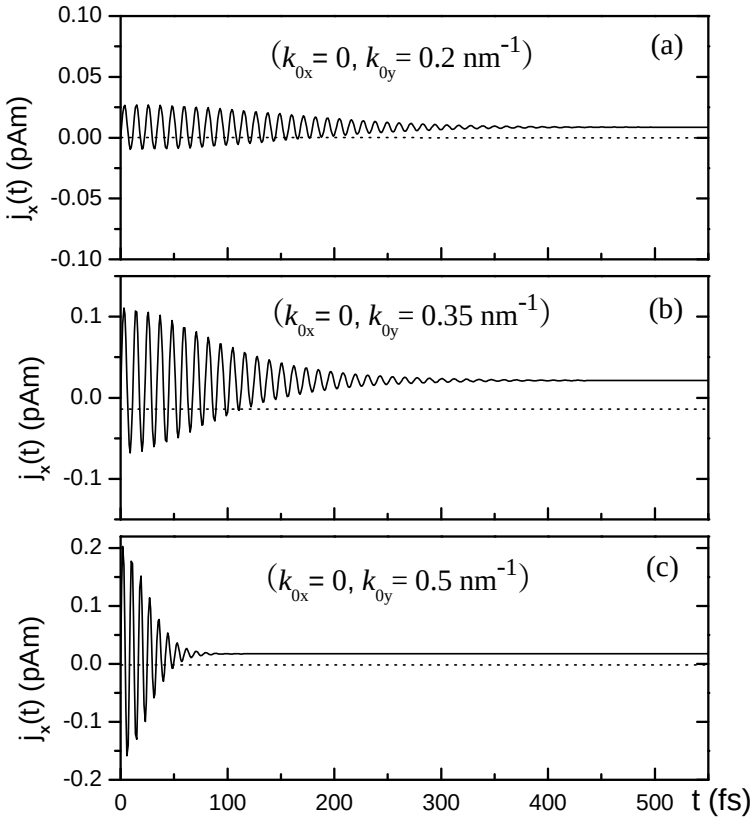

FIG. 4: Zitterbewegung of the x components of K- and K'-valley electric currents for different values of k_{0y} when $d = 30$ nm and $u = 0.5\gamma_1$. Since the x component is symmetric under the exchange of valley index (see Appendix B) no valley polarization occurs. For illustrative purpose, the high-energy case $k_{0y} = 0.5$ nm^{-1} ($E_0 = \hbar^2 k_0^2/2m^* \approx 170$ meV) is also plotted (see also Fig. 5).

uncertainty is $\Delta E \gtrsim \gamma_1$, which corresponds to the ZB frequency of $f_z \sim \gamma_1/h = 9.4\times10^{13}$ s^{-1}. From Fig. 2(c) the ZB frequency can be read off as $f_z \sim 9 \times 10^{13}$ s^{-1}, almost the same as the qualitative estimate. In fact, one can notice from Fig. 2 that the ZB frequency increases as u increases and the frequency in the biased BLG can be determined approximately by the bandgap, $f_z \sim \Delta/h \approx 2u/h$.

B. Effect of trigonal warping

We now investigate the effect of the TW distortion. In Figs. 4 and 5 we plot the x and y components of electric currents for different values of k_{0y} when $u = 0.5\gamma_1$. First, we observe that both the x and y components of the electric currents have the ZB oscillations. This is in contrast to the results of the unbiased BLG with isotropic energy dispersion in which only the x component

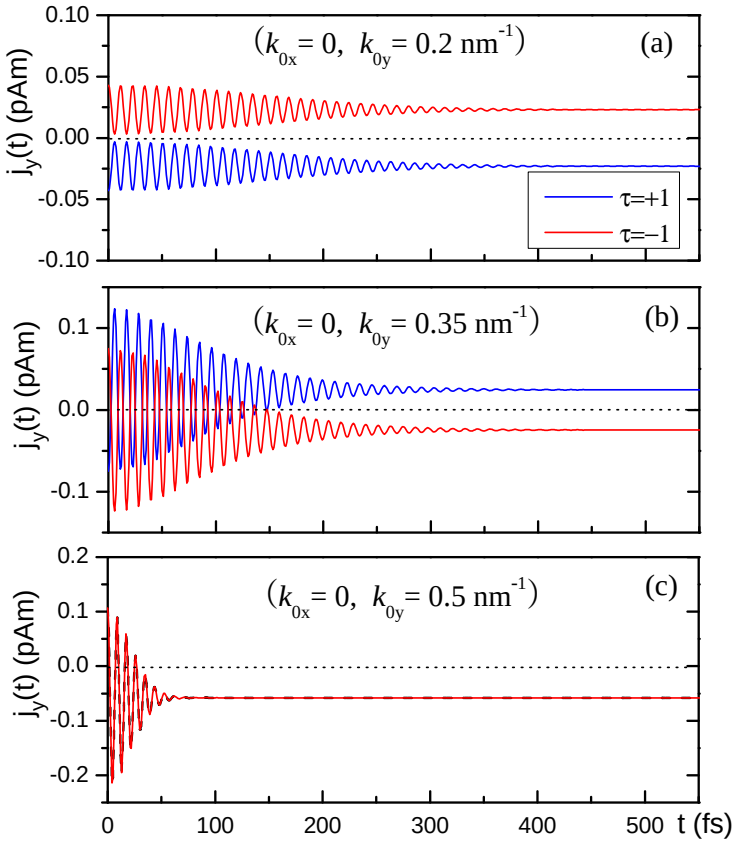

FIG. 5: (Color online) Zitterbewegung of the y components of K-valley (the blue lines) and K'-valley (the red lines) electric currents for different values of k_{0y} when $d = 30$ nm and $u = 0.5\gamma_1$. The polarization of the ZB's is (a) clear at small values of k_{0y}, (b) overlaps at intermediate values and (c) eventually disappear at large values (the red and dotted-blue lines).

displays the ZB oscillation.[19] The appearance of the y component is, of course, ascribed to the anisotropy of the eigenspectrum for which the TW term is responsible. If the TW term is neglected in the biased BLG one can easily see from Eq. (9) that only the y component can have the shift of oscillation center from the zero current. Thus, the existence of the shift in the x component (Fig. 4) can also be considered as a consequence of the anisotropic property.

The most notable feature from the results is that the ZB's of the y component (Fig. 5) at K and K' valleys are split due to the symmetry breaking TW distortion, that is, valley-polarized ZB's arise; the absence of polarization in the x component can be illustrated by the symmetric property of $v_{\tau x}(\boldsymbol{k}, t)$ in Eq. (9) under the exchange of valley index, which is shown in Appendix B. From Fig. 5(a), at small values of k_{0y}, the K-valley (the blue lines) and K'-valley (the red lines) ZB's

are completely polarized to negative and positive values, respectively; the oscillation amplitude is, however, small because of the small initial mean momentum corresponding to $k_{0y} = 0.2$ nm^{-1}. As k_{0y} increases, the center of the K-valley (K'-valley) ZB oscillation is switched from negative (positive) value to positive (negative) value; thus at certain value of k_{0y} (~ 0.29 nm^{-1}) minimum polarization occurs. Since the amplitude of the ZB oscillation becomes larger as k_{0y} is increased the two polarized ZB oscillations overlap each other for small initial times as can be seen from Fig. 5(b). For illustrative purpose we have also plotted the case $k_{0y} = 0.5$ nm^{-1} ($E_0 = \hbar^2 k_{0y}^2/2m^* \approx$ 170 meV) in Fig. 5(c). In this case the polarization disappears due to the loss of anisotropy at high energies, and the decay time reduces back to small value due to the large initial mean momentum; as one can see from Fig. 1(b), at large values of k, the slopes of the biased and unbiased cases become the same and steep to give large relative velocity.

Although the polarization effect does not occur in the x component the 2D electric current $\boldsymbol{j}_\tau(t) = j_{\tau x}(t)\mathbf{e}_x + j_{\tau y}(t)\,\mathbf{e}_y$ should be polarized due to the polarization in the y component. Since the ZB oscillation is transient these polarized currents will have constant values at large times which are determined by the constant velocities v_{x0} and v_{y0} in Eq. (9). In fact, the constant part of the average velocity $\boldsymbol{v}_\tau(t)$ is

$$\begin{aligned} \boldsymbol{v}_\infty^\tau &= \langle \boldsymbol{v} \rangle_{\tau+} + \langle \boldsymbol{v} \rangle_{\tau-} = \int d^2\boldsymbol{k}\, |A(\boldsymbol{k})|^2 \tau \frac{u - \epsilon_u}{E_\tau} \boldsymbol{v}_{g\tau}(\boldsymbol{k}) \\ &= \int d^2\boldsymbol{k}\, |A(\boldsymbol{k})|^2 \left[v_{x0}\mathbf{e}_x + v_{y0}\mathbf{e}_y \right], \end{aligned} \tag{12}$$

where $\boldsymbol{v}_\infty^\tau \equiv \lim_{t\to\infty} \boldsymbol{v}_\tau(t)$ and the second line can be obtained from the relation $\epsilon_u = \hbar^2 k^2/2m_u = u\lambda^2 k^2$ with $\lambda = \hbar v_F/\gamma_1$. Hence, the polarized constant currents are $\boldsymbol{j}_\tau = e\boldsymbol{v}_\infty^\tau$, whose components appear as the shifts of the ZB-oscillation centers shown in Fig. 2. As 2D currents, however, they occur at different directions, making an angle between them. The polarization angle between the two currents is $\theta_{KK'} = \arccos\left(\boldsymbol{j}_K \cdot \boldsymbol{j}_{K'}/|\boldsymbol{j}_K||\boldsymbol{j}_{K'}|\right)$, which are determined by the initial mean momentum $\hbar\boldsymbol{k}_0$ and the electric field; the effect of field on the polarization arises through the anisotropy of the eigenspectrum. As numerical examples, evaluating the average constant velocities from Eq. (12) when $u = 0.5\gamma_1$, we have $\theta_{KK'} \approx 140^\circ$ for $k_{0y} = 0.2$ nm^{-1} ($E_0 \approx 27$ meV) and $\theta_{KK'} \approx 100^\circ$ for $k_{0y} = 0.35$ nm^{-1} ($E_0 \approx 83$ meV). Since the x component is not polarized the directions of $\boldsymbol{j}_K$ and $\boldsymbol{j}_{K'}$ are symmetric about the x axis and each current makes an angle of $\theta_{KK'}/2$ from the x axis. To detect these polarized constant currents as well as the ZB oscillations experimentally, one may use the scanning probe microscopy which can map the currents as conductance image of the electron flows along the two polarization directions symmetric about the x axis.[41,42] As we have il-

lustrated in Fig. 1(a) the eigenspectrum is highly anisotropic within the energy range of $E \lesssim 0.1$ eV (i.e., $k_{0y} \lesssim 0.4$ nm^{-1}) (see the contour for $E = 0.25\gamma_1$).[43] Thus, the valley-polarized ZB oscillations with polarized constant currents at large times should be anticipated for the low-energy electrons in the biased BLG.

Finally, we recapitulate the combined effects of the TW distortion and the electric field. In order to observe the ZB it is preferable to have a long decay time and large oscillation amplitude of the electric current. It is also desirable to have large polarization angle for appreciable valley-polarized ZB's. Since the TW term is fixed by γ_3 controllable parameters are the bandgap parameter u and the initial mean momentum $\hbar\boldsymbol{k}_0$. As demonstrated above the amplitude of ZB oscillation is mainly determined by $\hbar\boldsymbol{k}_0$. On the other hand, the decay time and the polarization angle are controlled by both u and $\hbar\boldsymbol{k}_0$. Within the valid range of energy and the tunability of bandgap the results shown in Figs. 4(b) and 5(b) are close to an optimum situation. Combining these effects and considering the non-zero shifts of the oscillation centers we can expect, in the biased BLG with TW, valley-polarized transient ZB's of electric current with longer decay time which eventually converge to two valley-polarized constant electric currents at large times.

IV. SUMMARY

In summary, by investigating the effects of the trigonal warping and external electric field on the Zitterbewegung in a bilayer graphene, we found that (1) the decay time of the transient ZB can be controlled by tuning the bandgap with the applied electric field and (2) valley-polarized ZB's exist due to the symmetry breaking TW energy distortion. Within the range of the tunability of bandgap the decay time increases as the bandgap is increased. The behind mechanism of lengthening of the decay time is the decrease of average relative velocity between the conduction- and valence-band wave packets due to the slower group velocities in the presence of bandgap. The valley polarization of ZB produces two highly oscillating electric currents at different directions, and their polarization angle is determined by the initial mean momentum of electron wave packet and the applied electric field. Because of the transient character the ZB oscillations disappear at large times and two polarized constant electric currents are left. These constant currents can exist only in the presence of electric field, exhibiting another character of the ZB in the biased BLG. The valley-polarized ZB's of low-energy electrons in BLG should be expected in the valid energy range.

Acknowledgments

Daekil Park's research was supported by the Kyungnam University Research Fund, 2013.

Appendix A: velocity operator

Here we present the explicit expression of the velocity operator $\hat{\boldsymbol{v}}$ in Eq. (7). Using the momentum representation the commutator can be written as

$$\hat{\boldsymbol{v}} = \frac{1}{i\hbar}\left[i\hbar\nabla_{\boldsymbol{p}}, \hat{\mathcal{H}}(\boldsymbol{p})\right], \tag{A1}$$

where $\nabla_{\boldsymbol{p}} = \partial_{p_x}\mathbf{e}_x + \partial_{p_y}\mathbf{e}_x$ and $\hat{\mathcal{H}}(\boldsymbol{p})$ is given in Eq. (1). Performing the differentiations with respect to p_x and p_y it can be expressed as

$$\begin{aligned}
\hat{\boldsymbol{v}} &= \sigma_x\hat{\mathbf{v}}_x + \sigma_y\hat{\mathbf{v}}_y + \sigma_z\hat{\mathbf{v}}_z \\
\hat{\mathbf{v}}_x &= \left(-\tau\frac{\hat{\pi}}{m^*} + \tau v_3\right)\mathbf{e}_x \\
\hat{\mathbf{v}}_y &= -\left(\tau\frac{\hat{\pi}^\dagger}{m^*} + \tau v_3\right)\mathbf{e}_x \\
\hat{\mathbf{v}}_z &= -\tau\frac{1}{m_u}\left(\hat{p}_x\mathbf{e}_x + \hat{p}_y\mathbf{e}_y\right),
\end{aligned} \tag{A2}$$

where σ_i $(i = x, y, z)$ are the 2×2 Pauli matrices.

Appendix B: Valley dependence of $\boldsymbol{v}_\tau(t)$ and $\boldsymbol{v}^\tau_{rel}$

Since the average velocity (and hence the electric current) in Eq. (8) depends on the valley index τ it is useful to express the valley-dependent relations of the components of the velocity. We begin with the valley dependency of the eigenspectrum E_τ. From Eq. (2) it can written as

$$E_\tau(\boldsymbol{q}) = \gamma_1\left[(q^2+r^2)q^2 + \alpha^2(1-q^2)^2 - 2\tau r(4q_x^2 - 3q^2)q_x\right]^{1/2}, \tag{B1}$$

where, for notational convenience, we have introduced following dimensionless quantities, with $q^2 = q_x^2 + q_y^2$,

$$q_{x,y} = (\hbar v_F/\gamma_1)\,k_{x,y}, \quad \alpha = u/\gamma_1, \quad r = \gamma_3/\gamma_0.$$

The x and y components of the momentum-dependent group velocity $\boldsymbol{v}_{g\tau}(\boldsymbol{k})$ are then expressed as, with the replacement of $(1/\hbar)\nabla_{\boldsymbol{k}} E_\tau(\boldsymbol{k}) \rightarrow (v_F/\gamma_1)\nabla_{\boldsymbol{q}} E_\tau(\boldsymbol{q})$,

$$
\begin{aligned}
v_{g\tau x}(\boldsymbol{q}) &= \frac{\gamma_1 v_F}{E_\tau}\left[\left(2q^2 + r^2 - 2\alpha^2(1-q^2)\right)q_x - 3\tau r(q_x^2 - q_y^2)\right] \\
v_{g\tau y}(\boldsymbol{q}) &= \frac{\gamma_1 v_F}{E_\tau}\left[2q^2 + r^2 - 2\alpha^2(1-q^2) + 6\tau r q_x\right]q_y.
\end{aligned}
\tag{B2}
$$

For the choice of the Gaussian wave packet with initial mean momentum $\hbar\boldsymbol{k}_0 = (0, \hbar k_{0y})$ (i.e., $\boldsymbol{q}_0 = (0, q_{0y})$) the x component is a symmetric function of k_x (i.e, q_x) about the origin. Thus, we look into the q_x dependence of the above quantities. One can easily see

$$
E_\tau(-q_x) = E_{-\tau}(q_x), \tag{B3}
$$

from which it follows that

$$
v_{g\tau x}(-q_x) = -v_{g(-\tau)x}(q_x), \quad v_{g\tau y}(-q_x) = v_{g(-\tau)x}(q_x). \tag{B4}
$$

Using these relations it can be shown that the integrands $v_{\tau x}(\boldsymbol{k}, t)$ and $v_{\tau y}(\boldsymbol{k}, t)$ in Eq. (8) satisfy, using the dimensionless quantity $\boldsymbol{q}$,

$$
\begin{aligned}
v_{\tau x}(-q_x, q_y, t) &= v_{-\tau x}(q_x, q_y, t) = v_{-\tau x}(\boldsymbol{q}, t), \\
v_{\tau y}(-q_x, q_y, t) &= -v_{-\tau y}(q_x, q_y, t) = -v_{-\tau y}(\boldsymbol{q}, t).
\end{aligned}
\tag{B5}
$$

Consequently, the x and y components of the average velocity have the following relations, using the notations $\tau = +1 = K$ and $\tau = -1 = K'$,

$$
v_{K'x}(t) = v_{Kx}(t), \quad v_{K'y}(t) = -v_{Ky}(t). \tag{B6}
$$

Thus, the x component is symmetric but the y component is antisymmetric under the exchange of valley index. This explains why the x components of the electric currents in Figs. 2 and 4 display no valley polarization, while the y components in Fig. 5 are polarized with valley.

The same argument can be applied to the average relative velocity $\boldsymbol{v}^\tau_{rel}$ in Eq. (11). In this case, since the integrand is given by the gradient of the eigenspectrum E_τ, using the relations in Eq. (B2) one can easily show

$$
v^{K'}_{rel\,x} = -v^{K}_{rel\,x}\,, \quad v^{K'}_{rel\,y} = v^{K}_{rel\,y}\,. \tag{B7}
$$

This time the x component is antisymmetric but y component is symmetric under the exchange of valley index, which can be seen in Fig. 3; the x components are split into positive and negative values, while the y components are merged in one value. Finally, we remark that the above symmetry relations about $\boldsymbol{v}_\tau(t)$ and $\boldsymbol{v}^\tau_{rel}$ depend on the choice of the initial mean momentum $\hbar\boldsymbol{k}_0$.

---

* email: olnal@dankook.ac.kr

[1] E. Schrödinger, Sitzungsber. Preuss. Akd. Wiss., Phys. Math. Kl. **24**, 418 (1930).

[2] K. Huang, Am. J. Phys. **20**, 479 (1952).

[3] J. J. Sakurai, *Advanced Quantum Mechanics* (Addison-Wesley, Reading, MA, 1967), Chap. 3, Sec. 6.

[4] J. A. Lock, Am. J. Phys. **47**, 797 (1979).

[5] L. Ferrari and G. Russo, Phys. Rev. B **42**, 7454 (1990).

[6] W. Zawadzki, Phys. Rev. B **72**, 085217 (2005).

[7] W. Zawadzki, Phys. Rev. B **74**, 205439 (2006).

[8] W. Zawadzki and T. M. Rusin, J. Phys.: Condens. Matter **20**, 454208 (2008).

[9] J. Schliemann, D. Loss, and R. M. Westervelt, Phys. Rev. Lett. **94**, 206801 (2005); Phys. Rev. B **73**, 085323 (2006).

[10] J. Schliemann, New J. Phys. **10**, 034024 (2008).

[11] N. Shmueli, A. Yacobi, and J. Imry, Europhys. Lett. **29**, 711 (1995).

[12] D. Lurié and S. Cremer, Physica (Amsterdam) **50**, 224 (1970).

[13] J. Cserti and G. Dávid, Phys. Rev. B **74**, 172305 (2006).

[14] R. Winkler, U. Zülicke, and J. Bolte, Phys. Rev. B **75**, 205314 (2007).

[15] U. Zulicke, J. Bolte, and R. Winkler, New J. Phys. **9**, 355 (2007).

[16] M. I. Katsnelson, Eur. Phys. J. B **51**, 157 (2006).

[17] B. Trauzettel, Y. M. Blanter, and A. F. Morpurgo, Phys. Rev. B **75**, 035305 (2007).

[18] T. M. Rusin and W. Zawadzki, Phys. Rev. **B 76**, 195439 (2007).

[19] T. M. Rusin and W. Zawadzki, Phys. Rev. B **80**, 045416 (2009).

[20] K. S. Novoselov, A. K. Geim, S. V. Morozov, D. Jiang, M. I. Katsnelson, I. V. Grigorieva, S. V. Dubonos, and A. A. Firsov, Nature (London) **438**, 197 (2005).

[21] Y. B. Zhang, Y. W. Tan, H. L. Stoner, and P. Kim, Nature (London) **438**, 201 (2005).

[22] K. S. Novoselov, E. McCann, S. V. Morozov, V. I. Fal'ko, M. I. Katsnelson, U. Zeitler, D. Jiang, F.

Schedin, and A. K. Geim, Nat. Phys. **2**, 177 (2006).

[23] A. Castro Neto, F. Guinea, N. M. R. Peres, K. S. Novoselov, and A. K. Geim, Rev. Mod. Phys. **81**, 109 (2009).

[24] E. McCann and V. I. Fal'ko, Phys. Rev. Lett. **96**, 086805 (2006).

[25] C. J. Poole, Solid State Commun. **150**, 632 (2010).

[26] S. Park and H.-S. Sim, Phys. Rev. B **84**, 235432 (2011).

[27] C.-S. Park, Solid State Commun. **152**, 2018 (2012).

[28] E. McCann, D. S. L. Abergel, and V. I. Fal'ko, Solid State Commun. **143**, 110 (2007).

[29] E. McCann, Phys. Rev. B **74**, 161403(R) (2006).

[30] T. Ohta, A. Bostwick, T. Seyller, K. Horn, and E. Rotenberg, Science **313**, 951 (2006).

[31] E. V. Castro, K. S. Novoselov, S. V. Morozov, N. M. R. Peres, dosSantos J. M. B. Lopes, J. Nilsson, F. Guinea, A. K. Geim, and A. H. Castro Neto, Phys. Rev. Lett. **99**, 216802 (2007).

[32] E. V. Castro, N. M. R. Peres, J. M. B. Lopes dos Santos, F. Guinea, and A. H. Castro Neto, J. Phys.: Conference Series **129**, 012002 (2008).

[33] J. B. Oostinga, H. B. Heersche, X. Liu, A. F. Morpurgo, and L. M. K. Vandersypen, Nat. Mater. **7**, 151 (2008).

[34] G. M. Rutter, S. Jung, N. N. Klimov, D. B. Newell, N. B. Zhitenev, and J. A. Stroscio, Nat. Phys. **7**, 649 (2011).

[35] We use $v_F = (\sqrt{3}/2)a\gamma_0/\hbar = 9 \times 10^5$ m/s, where $a = 2.46 \times 10^{-10}$ m is the lattice constant.

[36] The theoretically predited value of the Lifshitz transition energy is given by $\epsilon^* = \gamma_1(\gamma_3/2\gamma_0)^2 \sim 1\,\text{meV}$,[24,28] but the experimentally observed value is $\epsilon^* \sim 6\,\text{meV}$.[37] Below this energy the spectrum splits into four Dirac cones each with linear dispersion.

[37] A. S. Mayorov, D. C. Elias, M. Mucha-Kruczynski, R. V. Gorbachev, T. Tudorovskiy, A. Zhukov, S. V. Morozov, M. I. Katsnelson, V. I. Fal'ko, A. K. Geim, and K. S . Novoselov, Science **333**, 860 (2011).

[38] In this paper we use the term *average velocity* in the sense of averaging over the momentum distribution of a wave packet to be distinguished from the group velocity $\boldsymbol{v}_{g\tau}(\boldsymbol{k})$ defined in Eq. (4).

[39] Notice that this choice corresponds to the initial packet in the pseudospinor state $(1\ 0)^T$.

[40] This is the case with the TW distortion. Without it, the decay time is $t = d/(\hbar k_{0y}/m^*) \approx 33$ fs using $v_F = 9 \times 10^5$ m/s.

[41] B. J. LeRoy, J. Phys.:Condens. Matter **15**, R1853 (2003).

[42] Vadim V. Cheianov, Vladmir Fal'ko, and B. L. Altshuler, Science **315**, 1252 (2007).

[43] For the maximum case of $u = 0.5\gamma_1$ the energy contours become less anisotropic than the case $u = 0.25\gamma_1$ plotted in the figure. However, even in this case the low-energy contours, beonging to the valid energy range, render high anisotropy to produce the valley-polarized ZB's as shown in the Fig. 5(b).